Angle-resolved photoemission in doped charge-transfer Mott insulators

A. S. Alexandrov and C. J. Dent
Department of Physics, Loughborough University, Loughborough LE11 3TU, United Kingdom
(Received 10 May 1999)

A theory of angle-resolved photoemission (ARPES) in doped cuprates and other charge-transfer Mott insulators is developed taking into account the realistic (LDA+U) band structure, (bi)polaron formation due to the strong electron-phonon interaction, and a random-field potential. In most of these materials, the first band to be doped is the oxygen band inside the Mott-Hubbard gap. We derive the coherent part of the ARPES spectra with the oxygen hole spectral function calculated in the noncrossing (ladder) approximation and with the exact spectral function of a one-dimensional hole in a random potential. Some unusual features of ARPES, including the polarization dependence and spectral shape in $YBa_2Cu_3O_7$ and $YBa_2Cu_4O_8$, are described without any Fermi surface, large or small. The theory is compatible with the doping dependence of kinetic and thermodynamic properties of cuprates as well as with the *d*-wave symmetry of the superconducting order parameter. [S0163-1829(99)00146-0]

I. INTRODUCTION

The concept of polarons led to the discovery of the copper oxide superconductors. The expectation was that if an electron and a surrounding lattice distortion with a high effective mass can travel through the lattice as a whole, and a strong electron-phonon coupling exists, the perovskite insulator could be turned into a high-temperature superconductor.[1] In this paper we develop the theory of angle-resolved photoemission (ARPES) in doped charge-transfer Mott insulators based on the bipolaron theory,[2,3] which describes some unusual ARPES features of high-T_c $YBa_2Cu_3O_{7-\delta}$ (Y123), $YBa_2Cu_4O_8$ (Y124), and a few other materials.

ARPES data in cuprates remains highly controversial.[4] One of the surprising features is a *large* Fermi surface claimed to exist in a wide range of doping fitting well the local-density approximation (LDA) band structures in the earlier studies. This should evolve with doping as $(1-x)$ in a clear contradiction with low-frequency kinetics and thermodynamics (see, for example, Refs. 5–10), which show an evolution proportional to x in a wide range of doping including the overdoped region[9,11] (x is the number of holes introduced by doping). Now it is established, however, that there is a normal-state (pseudo)gap in ARPES and tunneling, existing well above T_c,[12,13] so that some segments of a ''large Fermi surface'' are actually missing.[14] The temperature and doping dependence of the gap still remain a subject of controversy. While kinetic,[9] thermodynamic,[10,16] tunneling,[13] and some ARPES (Refs. 14 and 15) data suggest that the gap opens at any relevant temperature in a wide range of doping, other ARPES studies[17–19] claim that it exists only in underdoped samples below a characteristic temperature T^*.

Perhaps the most intriguing feature of ARPES is the extremely narrow and intense peak lying below the Fermi energy, which is most clearly seen near the Y and X points in Y124,[20] Y123,[21] and more recently in $La_{2-x}Sr_xCuO_4$.[22] Its angular dependence and spectral shape as well as the origin of the featureless (but dispersive) background remain unclear. Some authors[20] refer to the peak as an extended van Hove singularity (evHs) arising from the plane (CuO_2) strongly correlated band. They also implicate the resulting (quasi-) one-dimensional (1D) density-of-states singularity as a possible origin for the high transition temperature. However, recent polarized ARPES studies of untwinned Y123 crystals of exceptional quality[21] unambiguously refer to the peak as a narrow resonance arising primarily from the quasi-1D CuO_3 chains in the buffer layers rather than from the planes. Also, careful analysis of the Eliashberg equations shows that the van Hove singularity can hardly be the origin of high T_c, in sharp contrast with a naive weak-coupling estimate. Interestingly, a very similar narrow peak was observed by Park *et al.*[23] in high-resolution ARPES near the gap edge of the cubic *semiconductor* FeSi with no Fermi surface at all.

In this paper we take the view that cuprates and many other transition-metal compounds are charge-transfer Mott-Hubbard insulators at *any* level of doping[24] as established in the ''LDA+U'' band-structure calculations for cuprates and manganites[25] suggesting the single-particle density of states shown in Fig. 1. This means that the first band to be doped is the oxygen band lying within the Hubbard gap, Fig. 1. The strong on-site repulsion on copper (U) normally does not allow for the occurrence of a well-defined quasiparticle peak in the d band within the LDA+U approximation. However, the oxygen band, which is found inside the Hubbard gap,

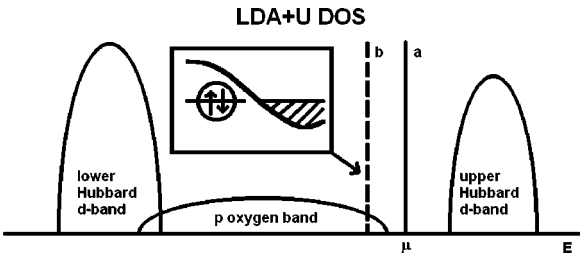

FIG. 1. Schematic LDA+U density of states. The chemical potential is pinned inside the charge-transfer gap (a) due to the bipolaron formation in underdoped cuprates. It might enter the oxygen band in overdoped cuprates (b) if the polaron band crosses the bipolaron one (inset).

Fig. 1, is less correlated and completely filled in an insulator. As a result, a single photoexited oxygen hole has well-defined quasiparticle properties in the absence of the electron-phonon (or spin-fluctuation) interaction. Strong coupling with high frequency phonons, unambiguously established for many oxides,[26] leads to the high-energy spectral features of an oxygen hole in an energy window about twice the Franck-Condon (polaronic) level shift E_p and to the band-narrowing effect.[2] On the other hand, the low-energy spectral function is influenced by the low-frequency thermal lattice, spin and random fluctuations. The latter can be described as ''Gaussian white noise.'' The *p*-hole polaron in oxides is almost one dimensional due to a large difference in the $pp\sigma$ and $pp\pi$ hopping integrals and effective ''one-dimensional'' localizitaion by the random potential as described in Ref. 27. This allows us to explain the narrow peak in the ARPES spectra with the spectral density $A(k,E)$ of a one-dimensional particle in a Gaussian white-noise potential.[28]

The electron-phonon interaction also binds holes into intersite oxygen bipolarons the size of a lattice constant.[2,29] The bipolaron density remains relatively low (below 0.15 per cell) at any relevant level of doping. The residual repulsive (Coulomb) hole polaron-bipolaron interaction[2] is strongly suppressed by the lattice polarization owing to a large static dielectric constant. As a result, the main role of hole bipolarons in ARPES is to pin the chemical potential inside the charge-transfer gap, half the bipolaron binding energy above the oxygen band edge, Fig. 1(a). This binding energy as well as the singlet-triplet bipolaron exchange energy are thought to be the origin of the normal-state pseudogaps, as proposed by one of us.[30] In particular, the non-Korringa temperature dependence of NMR (Ref. 30) and more recently the values and universal scaling with temperature of the uniform magnetic susceptibility[31,6,32] and electronic specific heat[32] were quantitatively described with bipolarons. In overdoped samples the (bi)polaronic carriers screen a static random potential and the electron low-frequency phonon interaction. Hence, the hole spectral function depends on doping. In particular, the bipolaron and polaron bands might overlap because the bipolaron binding energy becomes small,[31] so the chemical potential might enter the oxygen band, Fig. 1(b), and then a Fermi-level crossing might be seen in ARPES. The featureless background is explained as the phonon cloud of a small hole polaron, which spreads over a wide energy interval about $2E_p \simeq 1$ eV.

The same approach has been applied to the tunneling spectra.[33] As a result, the temperature independent gap and the anomalous gap/T_c ratio, injection/emission asymmetry both in magnitude and shape, zero-bias conductance at zero temperature, the spectral shape inside and outside the gap region, temperature/doping dependence and ''dip-hump'' structure of the tunneling conductance were described. It is clearly compatible with the doping evolution of thermodynamic and kinetic properties because holes introduced by doping into the oxygen band are the only carriers in our theory. Moreover, the derived *bipolaron* energy dispersion with minima at the Brillouin-zone boundaries provides *d*-wave symmetry of the Bose-Einstein condensate[33] in agreement with phase-sensitive experiments.[34] It also provides a parameter-free expression for T_c in a few dozen cuprates, irrespective of the level of doping.[35,36]

Here we first derive the polaronic ARPES theory in Sec. II. Then, in Sec. III we apply the simplest noncrossing approximation for the self-energy and compare it with the exact result in Sec. IV. The experimental ARPES results, in particular, the angular dispersion, spectral shape, and polarization dependence, are compared with the theory in Sec. V. We conclude that the narrow peak in ARPES is an *intrinsic* polaron (oxygen) band found below the chemical potential by half of the bipolaron binding energy. We also arrive at the conclusion that the present experimental photoemission spectra can be understood with a small Fermi surface or even *without any* Fermi surface (depending on doping).

II. POLARONIC ARPES

The interaction of the crystal with the electromagnetic field of frequency ν is described by the Hamiltonian (in the dipole approximation)

$$H_{\rm int} = (8\pi I)^{1/2} \sin(\nu t) \sum_{\mathbf{k},\mathbf{k}'} (\mathbf{e}\cdot\mathbf{d}_{\mathbf{k},\mathbf{k}'}) c_{\mathbf{k}}^{\dagger} h_{\mathbf{k}'}^{\dagger} + \text{H.c.}, \qquad (1)$$

where I is the intensity of the radiation with the polarization $\mathbf{e}$ (we take $c=\hbar=k_B=1$), $\mathbf{k}$ is the momentum of the final state (i.e., of the photoelectron registered by the detector), $\mathbf{k}'$ is the (quasi)momentum of the hole remaining in the sample after the emission, and $c_{\mathbf{k}}^{\dagger}$ and $h_{\mathbf{k}'}^{\dagger}$ are their creation operators, respectively. For simplicity, we suppress the band index in $h_{\mathbf{k}'}^{\dagger}$. Due to the translational symmetry of the Bloch states, $|\mathbf{k}'\rangle \equiv u_{-\mathbf{k}'}(\mathbf{r})\exp(-i\mathbf{k}'\cdot r)$, there is a momentum conservation rule in the dipole matrix element,

$$d_{\mathbf{k},\mathbf{k}'} = d(\mathbf{k})\,\delta_{\mathbf{k}+\mathbf{k}',\mathbf{G}} \qquad (2)$$

with

$$d(\mathbf{k}) = ie(N/v_0)^{1/2} \nabla_{\mathbf{k}} \int_{v_0} e^{-i\mathbf{G}\cdot r} u_{\mathbf{k}-\mathbf{G}}(\mathbf{r})\, d\mathbf{r}, \qquad (3)$$

where $\mathbf{G}$ is a reciprocal-lattice vector, N the number of unit cells in the crystal of the volume Nv_0.

The Fermi Golden Rule gives the photocurrent to be

$$I(\mathbf{k},E) = 4\pi^2 I |\mathbf{e}\cdot d(\mathbf{k})|^2 \sum_{i,f} e^{\Omega+\mu N_i - E_i} |\langle f|h_{\mathbf{k}-\mathbf{G}}^{\dagger}|i\rangle|^2 \times \delta(E+E_f-E_i), \qquad (4)$$

where E is the binding energy, $E_{i,f}$ is the energy of the initial and final states of the crystal, and Ω,μ,N_i are the thermodynamic and chemical potentials and the number of holes, respectively. By definition the sum in Eq. (4) is $n(E)A(\mathbf{k}-\mathbf{G},-E)$, where the spectral function $A(\mathbf{k}-\mathbf{G},E) = (-1/\pi)\mathrm{Im}G^R(\mathbf{k}-\mathbf{G},E)$ is proportional to the imaginary part of the retarded Green function (GF) and $n(E)=[\exp(E/T)+1]^{-1}$, the Fermi distribution. In the following we consider temperatures well below the experimental energy resolution, so that $n(E)=1$ if E is negative and zero otherwise, and, for convenience, we put $\mathbf{G}=0$.

The spectral function depends on essential interactions of a single hole with the rest of the system. As we argued earlier[27] the most important interaction in oxides is the Fröh-

lich long-range electron-phonon interaction[37] of the oxygen hole with the *c*-axis polarized high-frequency phonons. This interaction results in self-trapped polarons.[38,39] The Fröhlich interaction is integrated out with the Lang-Firsov canonical transformation,[40] which is a multipolaron equivalent of a single-polaron displacement transformation.[41] With the quantum Monte Carlo (QMC) technique,[42] one can prove that this transformation, is practically exact for a long-range interaction in a wide region of the coupling strength, including the intermediate- and weak-coupling regime and in a wide range of the adiabatic ratio, ω/D (ω is the phonon frequency and D is the bandwidth). By applying the Lang-Firsov canonical transformation, the hole Matsubara GF is expressed as a convolution of the coherent polaron GF and the multiphonon correlation function,[3]

$$\mathcal{G}(\mathbf{k},\omega_n)=\frac{T}{N}\sum_{\omega_{n'},\mathbf{m},\mathbf{k}'}\frac{\sigma(\mathbf{m},\omega_{n'}-\omega_n)e^{i(\mathbf{k}-\mathbf{k}')\cdot\mathbf{m}}}{i\omega_{n'}-\xi_{\mathbf{k}'}}, \quad (5)$$

where the multiphonon correlation function, $\sigma(\mathbf{m},\tau)=T\Sigma_n e^{-i\Omega_n\tau}\sigma(\mathbf{m},\Omega_n)$, is found as

$$\sigma(\mathbf{m},\tau)=\exp\left(\frac{1}{2N}\sum_{\mathbf{q}}|\gamma(\mathbf{q})|^2 f_{\mathbf{q}}(\mathbf{m},\tau)\right). \quad (6)$$

Here

$$f_{\mathbf{q}}(\mathbf{m},\tau)=[\cos(\mathbf{q}\cdot\mathbf{m})\cosh(\omega_{\mathbf{q}}|\tau|)-1]\times\coth\frac{\omega_{\mathbf{q}}}{2T}+\cos(\mathbf{q}\cdot\mathbf{m})\sinh(\omega_{\mathbf{q}}|\tau|)$$

with $\mathbf{m}$ the lattice vector, $\omega_n=\pi T(2n+1)$, $n=0,\pm1,\pm2,\ldots$, and $\Omega_n=2\pi Tn$.

In the case of dispersionless phonons and a short-range (Holstein) interaction with a q independent matrix element [$\omega_{\mathbf{q}}=\omega$, $|\gamma(\mathbf{q})|^2=2g^2$], one can readily calculate the Fourier component of $\sigma(\mathbf{m},\tau)$ to obtain[3]

$$\mathcal{G}(\mathbf{k},\omega_n)=\frac{e^{-g^2}}{i\omega_n-\xi_{\mathbf{k}}}+\frac{e^{-g^2}}{N}\sum_{l=1}^{\infty}\frac{g^{2l}}{l!}\times\sum_{\mathbf{k}'}\left(\frac{n_{\mathbf{k}'}}{i\omega_n-\xi_{\mathbf{k}'}+l\omega}+\frac{1-n_{\mathbf{k}'}}{i\omega_n-\xi_{\mathbf{k}'}-l\omega}\right). \quad (7)$$

The Green's function of a polaronic carrier comprises two different contributions. The first coherent **k**-dependent term arises from the polaron band tunneling. The spectral weight of the coherent part is strongly (exponentially) suppressed as $Z=\exp(-g^2)$ and the effective mass is strongly enhanced, $\xi_{\mathbf{k}}=ZE_{\mathbf{k}}-\mu$ (we include the polaronic level shift into the chemical potential, μ). Here $E(\mathbf{k})$ is the bare (LDA+U) *hole* band dispersion. The second **k**-independent contribution describes the excitations accompanied by the emission and absorption of phonons. We believe that this term, $I_{\rm incoh}(E)$, is responsible for the asymmetric background in the optical conductivity and in the photoemission spectra of cuprates and manganites. We notice that its spectral density spreads over a wide energy range of about twice the polaron level shift $E_p=g^2\omega$. On the contrary, the coherent term shows an angular dependence in the energy range of the order of the polaron bandwidth $2w\equiv ZD$.

As we have discussed above, ARPES measures the imaginary part of the retarded GF multiplied by the Fermi-Dirac distribution function and by the square of the dipole matrix element. G^R is obtained from $\mathcal{G}(\mathbf{k},\omega_n)$ with a substitution $i\omega_n\to E+i0^+$. As a result, we obtain

$$I(\mathbf{k},E)\sim|d(\mathbf{k})|^2 n(E)Z\delta(E+\xi_{\mathbf{k}})+I_{\rm incoh}(E), \quad (8)$$

where $I_{\rm incoh}(E)$ is a structureless function of the binding energy, which spreads from about $-\omega$ down to $-2E_p$. Only in the extreme limit of a very strong electron-phonon coupling, where the polaron bandwidth is well below the phonon frequency, can multiphonon structure in $I_{\rm incoh}(E)$ be verified. It has actually been observed in the optical conductivity.[26]

The small Holstein polaron is very heavy except if the phonon frequency is extremely high.[27] In fact, oxides are ionic semiconductors where the long-range electron-phonon interaction dominates because of a poor screening. That leads to a much lighter, mobile small Fröhlich polaron (SFP).[27,42] It is easy to show[43] using Eqs. (5) and (6) that for any finite-radius interaction with a q-dependent matrix element the coherent part of ARPES spectra takes the same form as Eq. (8) but with a *different* spectral weight (Z) and effective-mass (Z') renormalization exponents. Also some **k** dependence of the *incoherent* background appears if the matrix element of the electron-phonon interaction depends on q.[44] Hence, in general,

$$I(\mathbf{k},E)\sim|d(\mathbf{k})|^2 n(E)Z\delta(E+\xi_{\mathbf{k}})+I_{\rm incoh}(\mathbf{k},E), \quad (9)$$

with the same $Z=\exp(-E_p/\omega)$ as in the case of the Holstein polaron but with the SFP bandwidth much less reduced, $\xi_{\mathbf{k}}=Z'E(\mathbf{k})-\mu$, where $Z'=\exp(-\gamma E_p/\omega)$. In general, one finds

$$\gamma=\sum_{\mathbf{q}}|\gamma(\mathbf{q})|^2[1-\cos(\mathbf{q}\cdot\mathbf{a})]\Big/\sum_{\mathbf{q}}|\gamma(\mathbf{q})|^2 \quad (10)$$

and $E_p=(1/2N)\Sigma_{\mathbf{q}}|\gamma(\mathbf{q})|^2\omega_{\mathbf{q}}$. The numerical coefficient γ might be as small as 0.4 (Ref. 42) and even smaller in the cuprates with the nearest-neighbor oxygen-oxygen distance less than the lattice constant, $\gamma\simeq0.2$,[27] which is precisely confirmed by exact QMC calculation of the small polaron mass.[42] On the one hand, this important result tells us that small polarons as well as intersite bipolarons are perfectly mobile and can account for the high-T_c values in cuprates.[35] On the other hand, the coherent spectral weight remains strongly suppressed in polaronic conductors, Eq. (9), because Z might be less than Z' by one or even a few orders of magnitude. These unusual SFP spectral features provide an explanation for the apparent discrepancy between a very small Drude weight and a relatively moderate mass enhancement, $m^*\sim3m_e-10m_e$ (depending on doping), of carriers in manganites[45,46] and cuprates. They also explain why the evHs observed in ARPES (Refs. 20–22) can hardly be seen in angle averaged photoemission. Indeed, the integrated spectral weight of the incoherent background is proportional to $(1-Z)$, Eq. (7). It turns out to be much larger than the coherent contribution, proportional to $Z\ll1$. Finally, the **k**-dependent *incoherent* background might obscure the experimental determination of the Fermi-level crossing. The precise assessment of its role involves somewhat lengthy computations, and it will be presented elsewhere.

FIG. 2. The noncrossing diagram for the self-energy. The dashed line corresponds to the random potential and (or) to the thermal lattice and spin fluctuations.

In the following we concentrate on the angular, spectral, and polarization dependence of the first coherent term, Eq. (9). The present experimental resolution[4] allows probing of the intrinsic damping of the coherent polaron tunneling. This damping appears due to the random field and low-frequency lattice and spin fluctuations described by the polaron self-energy $\Sigma_p(\mathbf{k},E)$, so that the coherent part of the spectral function is given by

$$A_p(\mathbf{k},E)=-(1/\pi)\times\frac{\mathrm{Im}\Sigma_p(\mathbf{k},E)}{[E+\mathrm{Re}\Sigma_p(\mathbf{k},E)-\xi_{\mathbf{k}}]^2+[\mathrm{Im}\Sigma_p(\mathbf{k},E)]^2}. \tag{11}$$

Hence, the theory of the narrow ARPES peak reduces to the determination of the self-energy of the coherent small hole polaron scattered by impurities, low-frequency deformation, and spin fluctuations.

III. SELF-ENERGY OF 1D HOLE IN THE NONCROSSING APPROXIMATION

Due to energy conservation, small polarons exist in the Bloch states at temperatures well below the optical-phonon frequency $T\ll\omega/2$ no matter how strong their interaction with phonons is.[40,47–49,2] This textbook result, known for a long time, has been questioned by some authors.[50] It has been shown[51] that the confusion is due to a profound misunderstanding of the strong-coupling expansion by those authors. The finite polaron self-energy appears only due to the (quasi)elastic scattering. First, we apply the simplest noncrossing (ladder) approximation to derive the analytical results, Fig. 2. Within this approximation the self-energy is $\mathbf{k}$ independent for a short-range scattering potential like the deformation or a screened impurity potential, so that

$$\Sigma_p(E)\sim\sum_{\mathbf{k}} G_p^R(\mathbf{k},E), \tag{12}$$

with $G_p^R(\mathbf{k},E)=[E-\xi_{\mathbf{k}}-\Sigma_p(E)]^{-1}$.

The oxygen polaron spectrum is parametrized in the tight-binding model as[27]

$$\xi_{\mathbf{k}}^{x,y}=2[t\cos(k_{x,y}a)-t'\cos(k_{y,x}a)+t_c\cos(k_z d)]-\mu. \tag{13}$$

If the oxygen hopping integrals in Eq. (13), reduced by the narrowing effect, are positive, the minima of the polaron bands are found at the Brillouin-zone boundary in X $(\pi,0)$ and Y $(0,\pi)$. The wave vectors corresponding to the energy minima belong to the stars with two prongs. Their group has only 1D representations. This means that the spectrum is degenerate with respect to the number of prongs of the star. The spectrum [Eq. (13)] belongs to the star with two prongs, and, hence, it is twofold degenerate.[36] The doublet is degenerate if the hole resides on the apical oxygen.[52] In general, the degeneracy can be removed due to the chains in the buffer layers of Y123 and Y124, so that the y-polaronic band corresponding to the tunneling along the chains might be the lowest one.

As mentioned above, the oxygen hole is (quasi-)one-dimensional due to a large difference between the oxygen hopping integrals for the orbitals elongated parallel to and perpendicular to the oxygen-oxygen hopping $t',t_c\ll t$. This allows us to apply a one-dimensional approximation, reducing Eq. (13) to two 1D parabolic bands near the X and Y points, $\xi_{\mathbf{k}}^{x,y}=k^2/2m^*-\mu$ with $m^*=1/2ta^2$ and k taking relative to $(\pi,0)$ and $(0,\pi)$, respectively. Then, the equation for the self-energy in the noncrossing approximation [Eq. (12)] takes the form:

$$\Sigma_p(\epsilon)=-2^{-3/2}[\Sigma_p(\epsilon)-\epsilon]^{-1/2} \tag{14}$$

for each doublet component. Here we introduce a dimensionless energy (and self-energy), $\epsilon\equiv(E+\mu)/\epsilon_0$ using $\epsilon_0=(D^2m^*)^{1/3}$ as the energy unit. The constant D is the second moment of the Gaussian white-noise potential, comprising thermal and random fluctuations as $D=2(V_0^2T/M+n_{im}v^2)$, where V_0 is the amplitude of the deformation potential, M is the elastic modulus, n_{im} is the impurity density, and v is the coefficient of the δ-function impurity potential. The solution is

$$\Sigma_p(\epsilon)=\frac{\epsilon}{3}-\left(\frac{1+i3^{1/2}}{2}\right)\left[\frac{1}{16}+\frac{\epsilon^3}{27}+\left(\frac{1}{256}+\frac{\epsilon^3}{216}\right)^{1/2}\right]^{1/3}-\left(\frac{1-i3^{1/2}}{2}\right)\left[\frac{1}{16}+\frac{\epsilon^3}{27}-\left(\frac{1}{256}+\frac{\epsilon^3}{216}\right)^{1/2}\right]^{1/3}. \tag{15}$$

While the energy resolution in the present ARPES studies is almost perfect,[4] the momentum resolution remains rather poor, $\delta>0.1\pi/a$. Hence, we have to integrate the spectral function, Eq. (11), with a Gaussian momentum resolution to obtain the experimental photocurrent,

$$I(\mathbf{k},E)\sim Z\int_{-\infty}^{\infty}dk'A_p(k',-E)\exp\left[-\frac{(k-k')^2}{\delta^2}\right]. \tag{16}$$

The integral is expressed in terms of $\Sigma_p(\epsilon)$ [Eq. (15)] and the tabulated error function $w(z)$ as

$$I(\mathbf{k},E)\sim-\frac{2Z}{\delta}\mathrm{Im}\{\Sigma_p(\epsilon)[w(z_1)+w(z_2)]\}, \tag{17}$$

where $z_{1,2}=[\pm k-i/2\Sigma_p(\epsilon)]/\delta$, $w(z)=e^{-z^2}\mathrm{erfc}(-iz)$, and $\epsilon=(-E+\mu)/\epsilon_0$. This photocurrent is plotted as dashed lines in Fig. 3 for two momenta, $k=0.04\pi/a$ (almost Y or X points of the Brillouin zone) and $k=0.3\pi/a$. The chemical potential is placed in the charge-transfer gap below the bottom of the hole band, $\mu=-20$ meV, the momentum resolution is taken as $\delta=0.28\pi/a$, and the damping $\epsilon_0=19$ meV.

The imaginary part of the self-energy [Eq. (15)] disappears below $\epsilon=-3/2^{5/3}\simeq-0.9449$. Hence, this approximation gives a well-defined gap rather than a pseudogap. Actu-

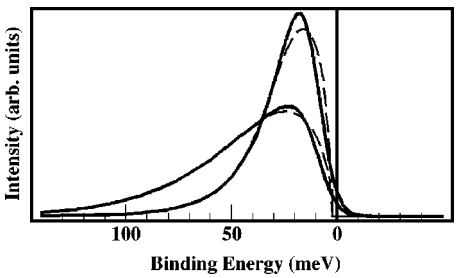

FIG. 3. The polaron spectral function, integrated with the momentum resolution function for two angles, $k=0.04\pi/a$ (upper curves) and $k=0.30\pi/a$, with the damping $\epsilon_0=19$ meV, the momentum resolution $\delta=0.28\pi/a$, and the polaron mass $m^*=9.9m_e$. The bipolaron binding energy $2|\mu|=40$ meV. The dashed curves are the spectral density integrated with the momentum resoltion in the noncrossing approximation.

ally, the noncrossing approximation fails to describe the localized states inside the gap (i.e., the Lifshitz tail of the density of states). One has to go beyond the simple ladder, Fig. 2, to describe the single-electron tunneling inside the gap[33] and the ARPES spectra at very small binding energy.

IV. EXACT SPECTRAL FUNCTION OF 1D HOLE

The exact spectral function for a one-dimensional particle in a random Gaussian white-noise potential was derived by Halperin[28] and the density of states by Frisch and Lloyd.[53] Halperin derived two pairs of differential equations from whose solutions the spectral function of a ''Schrodinger'' particle (i.e., in the effective-mass approximation) and of a ''discrete'' particle (tight-binding approximation) may be calculated. The QMC polaronic bandwidth is about 100 meV or larger,[42] which allows us to apply the Schrodinger particle spectral function, given by[28]

$$A_p(k,\epsilon)=4\int_{-\infty}^{\infty}p_0(-z)\mathrm{Re}p_1(z)dz, \tag{18}$$

where $p_{0,1}(z)$ obey the two differential equations

$$\left[\frac{d^2}{dz^2}+\frac{d}{dz}(z^2+2\epsilon)\right]p_0=0, \tag{19}$$

and

$$\left[\frac{d^2}{dz^2}+\frac{d}{dz}(z^2+2\epsilon)-z-ik\right]p_1+p_0=0, \tag{20}$$

with boundary conditions

$$\lim_{z\to\infty} z^{2-n}p_n(z)=\lim_{z\to-\infty} z^{2-n}p_n(z), \tag{21}$$

where k is measured in units of $k_0=(D^{1/2}m^*)^{2/3}$. The first equation may be integrated to give

$$p_0(z)=\frac{\exp(-z^3/3-2z\epsilon)\int_{-\infty}^{z}\exp(u^3/3+2u\epsilon)du}{\pi^{1/2}\int_0^{\infty}u^{-1/2}\exp(-u^3/12-2u\epsilon)du}. \tag{22}$$

The equation for $p_1(z)$ has no known analytic solution and, hence, must be solved numerically. There is, however, an asymptotic expression for $A_p(k,\epsilon)$ in the tail where $|\epsilon|\gg 1$:

$$A_p(k,\epsilon)\sim 2\pi(-2\epsilon)^{1/2}\exp\left[-\frac{4}{3}(-2\epsilon)^{3/2}\right]\times\cosh^2\left[\frac{\pi k}{(-8\epsilon)^{1/2}}\right]. \tag{23}$$

In practice, for computational efficiency we use the exact spectral density for $-1.4\leqslant\epsilon<1$, and outside this range we use the asymptotic result for $\epsilon<-1.4$ [Eq. (23)] and the non-crossing approximation for $\epsilon\geqslant 1$, where they are almost indistinguishable from the exact result on the scale of the diagrams plotted here.

The result for $A_p(k,-E)$ integrated with the Gaussian momentum resolution is shown in Fig. 3 for two values of the momentum (solid lines). Quite differently from the noncrossing approximation the exact spectral function (averaged with the momentum resolution function) has the Lifshitz tail due to the states localized by disorder within the normal-state gap. However, besides this tail the noncrossing approximation gives very good agreement, and for binding energy greater than about 30 meV, it is practically exact. Owing to the screening of the static (or low-frequency) random potential, (bi)polarons can reduce the characteristic length of the tail, ϵ_0. This familiar tendency towards delocalization of carriers with doping[54] in semiconductors should be distinguished from that in low-dimensional disordered metals where the interaction effects also favor some delocalization.[55]

The cumulative density of states (DOS),

$$N_p(\epsilon)=(2\pi)^{-1}\int_{-\infty}^{\epsilon}d\epsilon'\int_{-\infty}^{\infty}dkA_p(k,\epsilon'), \tag{24}$$

is expressed analytically[53] in terms of the tabulated Airy functions $Ai(x)$ and $Bi(x)$ as

$$N_p(\epsilon)=\pi^{-2}[Ai^2(-2\epsilon)+Bi^2(-2\epsilon)]^{-1}. \tag{25}$$

The DOS $dN_p(\epsilon)/d\epsilon$ fits well the voltage-current tunneling characteristics of cuprates.[33]

V. THEORY OF ARPES IN Y124 AND Y123

With the polaronic doublet [Eq. (13)] placed above the chemical potential, we can quantitatively describe high-resolution ARPES in Y123 (Ref. 21) and Y124 (Ref. 20). First, we explain the experimentally observed polarization dependence of the intensity near Y and X.[21] The Bloch periodic function $u_{\mathbf{k}}(\mathbf{r})$ can be expressed in terms of the Wannier orbitals $w(\mathbf{r})$ as

$$u_{\mathbf{k}}(\mathbf{r})=N^{-1/2}\sum_{\mathbf{m}} e^{i\mathbf{k}\cdot(\mathbf{m}-\mathbf{r})}w(\mathbf{r}-\mathbf{m}). \tag{26}$$

Then the dipole matrix element is given by the derivative of the Fourier component of the atomic (Wannier) orbital, $f_{\mathbf{k}}\equiv v_0^{-1/2}\int d\mathbf{r}w(\mathbf{r})\exp(i\mathbf{k}\cdot\mathbf{r})$, as

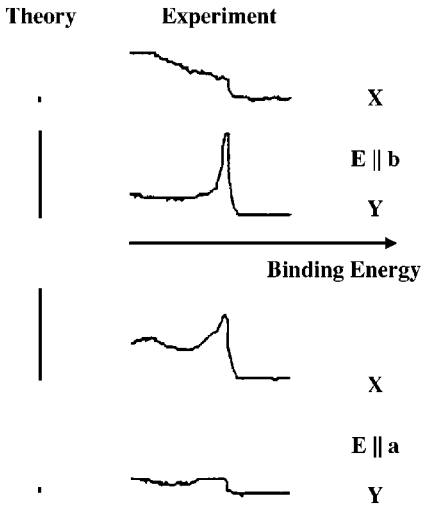

FIG. 4. Polarization dependence of the ARPES peak in Y123 (Ref. 21) near X and Y points compared with the theory.

$$d(\mathbf{k}) = i(\mathbf{e}\cdot\nabla_{\mathbf{k}})f_{\mathbf{k}}. \tag{27}$$

To estimate $f_{\mathbf{k}}$, we approximate the x,y oxygen orbitals contributing to the x and y polaronic bands, respectively, with $w_x(\mathbf{r}) = (1/8a_0^3\pi)^{1/2}(x/2a_0)\exp(-r/2a_0)$ and $w_y(\mathbf{r}) = (1/8a_0^3\pi)^{1/2}(y/2a_0)\exp(-r/2a_0)$. As a result, we obtain for the x orbital,

$$\frac{\partial f_{\mathbf{k}}}{\partial k_x} = (8a_0^3\pi/v_0)^{1/2}a_0\{[(ka_0)^2+1/4]^{-3} - 6(k_x a_0)^2[(ka_0)^2+1/4]^{-4}\} \tag{28}$$

and

$$\frac{\partial f_{\mathbf{k}}}{\partial k_{y,z}} = -6(8a_0^3\pi/v_0)^{1/2}a_0^3 k_x k_{y,z}[(ka_0)^2+1/4]^{-4}. \tag{29}$$

Here $\mathbf{k}$ is the photoelectron momentum, and a_0 is the size of the Wannier function. For the case of y orbital, one should interchange x and y. Near the X and Y points of the Brillouin zone, we have $|k_{y,x}| \ll k$, respectively. Then it follows from Eqs. (28) and (29) that the ARPES peak should be seen at X and almost disappear at Y if the photons are polarized along the x direction, i.e., $\mathbf{e}\|\mathbf{a}$. If the polarization is along the y direction ($\mathbf{e}\|\mathbf{b}$), the peak appears at Y and almost disappears at X. Precisely this behavior is observed in ARPES spectra obtained using polarized photons,[21] Fig. 4. We also notice a very strong dependence of the dipole matrix element [Eq. (28)] on the photon energy $d \sim \nu^{-3}$ at large ν. Hence, it is not surprising if the ARPES peak disappears at large ν as has been recently observed.[56]

The exact 1D polaron spectral function, Eq. (18), integrated with the experimental momentum resolution (shown in Fig. 5), provides a quantitative fit to the ARPES spectra in Y124 along the Y-Γ direction [Fig. 2(a) of Ref. 20]. The angular dispersion is described with the polaron mass $m^* = 9.9m_e$ in agreement with the Monte Carlo calculations of the SFP mass.[42] The spectral shape is reproduced well with $\epsilon_0 = 19$ meV, Fig. 6, in close agreement with the value of this

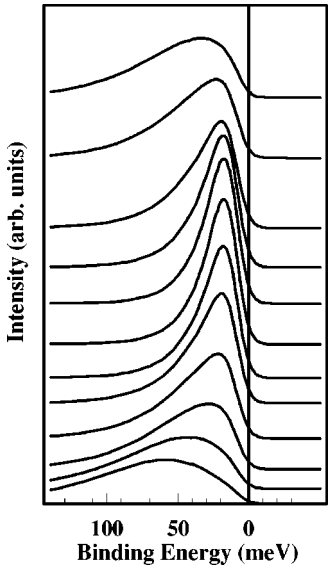

FIG. 5. Theoretical ARPES spectra for Y-Γ direction. Parameters are those of Fig. 3. The theory provides a quantitative fit to experiment [Fig. 2(a) of Ref. 20] in this scanning direction.

parameter found in tunneling experiments.[33] That yields an estimate of the polaron scattering rate, which appears to be smaller than the polaron bandwidth (about 100 meV or larger), in agreement with the notion[27] that many high-T_c cuprates are in the clean limit. There is also quantitative agreement between theory (Fig. 7) and experiment [Fig. 3(a) yof Ref. 20] in the perpendicular direction Y-S, in a restricted region of small k_x, where almost no dispersion is observed ary ound Y. Slight dispersion in the Y-S direction towards the chemical potential might be due to a negative t' in Eq. (13).

However, there is a significant loss of the energy-integrated intensity along both directions, Fig. 8, which the theoretical spectral function alone cannot account for. The energy-integrated ARPES spectra obey the sum rule,

$$\int_{-\infty}^{\infty} dE I(\mathbf{k},E) \sim |d(\mathbf{k})|^2 n_{\mathbf{k}}, \tag{30}$$

where $n_{\mathbf{k}} = \langle h_{\mathbf{k}} h_{\mathbf{k}}^{\dagger}\rangle$. If the dipole matrix element is almost k independent, and the chemical potential is pinned well inside the charge-transfer gap, so that $n_{\mathbf{k}} = 1$ this integral would be

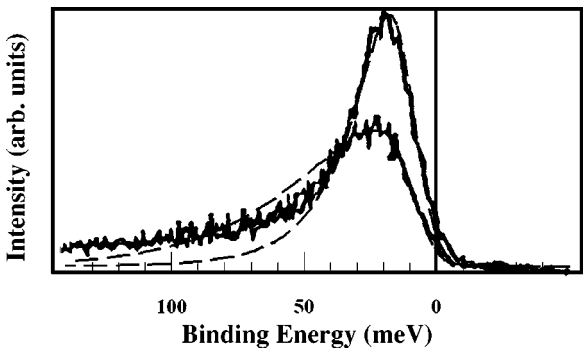

FIG. 6. Theoretical fit (dashed lines) to two experimental ARPES curves corresponding to $k = 0.04\pi/a$ (upper curves) and $k = 0.30\pi/a$ (momenta are measured relative to the Y point of the Brillouin zone).

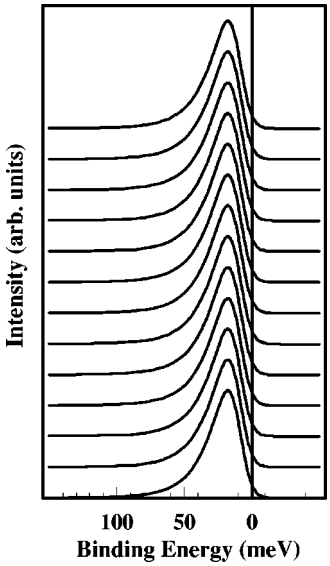

FIG. 7. Theoretical ARPES spectra in Y124 for Y-S direction. The theoretical fit agrees well with experiment [Fig. 3(a) of Ref. 20] in a restricted range of k_x near the Y point, and outside this range the theoretical peaks are somewhat higher than in experiment.

k independent as well. This is not the case for Y124, no matter what the scanning direction is, Fig. 8. Therefore, we have to conclude that either the dipole matrix element is **k** dependent or (and) the oxygen band is strongly correlated (in the Mott-Hubbard sense). As we have mentioned above, the incoherent background of SFP is angle dependent as well, which might contribute to the intensity loss.

The rapid loss of the integrated intensity in the Y-S direction was interpreted by Randeria and Campuzano [18] as a Fermi-surface crossing. While a Fermi-surface crossing is not incompatible with our scenario (see Fig. 1 inset), we do not believe that it has really been observed in Y124. First of all these authors suppressed a few experimental curves in the Y-Γ direction, which prevented them from observing the intensity loss in this ''dielectric'' direction, where there is obviously no Fermi-surface crossing. This loss of intensity along Y-Γ tells us that the intensity loss might be due to the matrix element rather than to the Fermi-surface crossing in both directions. This is confirmed by our observation of a similar rapid loss of the intensity in a *dielectric*, FeSi (Ref. 23) (see Fig. 9) with no Fermi surface at all. The peaks in the

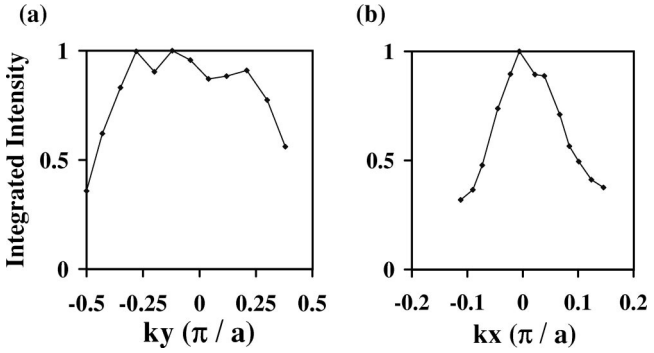

FIG. 8. The energy-integrated ARPES intensity in Y124 in the Y-Γ (a) and Y-S (b) directions. Momenta are measured relative to the Y point of the Brillouin zone.

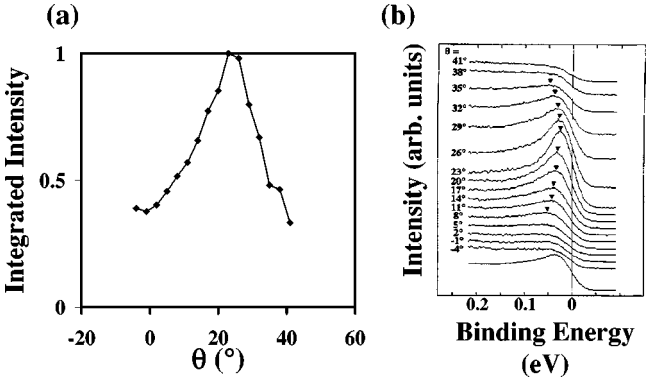

FIG. 9. (a) The energy-integrated ARPES intensity in FeSi (Ref. 23) as a function of the analyzer angle. The spectra are shown in (b).

Y-S direction are all 15 meV or more below the Fermi level. At a temperature of 1 meV, if the loss of spectral weight were due to a Fermi-surface crossing, one would expect the peaks to approach much closer to the Fermi level. Also the experimental spectral shape of the intensity at $\mathbf{k}=\mathbf{k}_F$ is incompatible with any theoretical scenario, including different marginal Fermi-liquid models, Fig. 10. The spectral function on the Fermi surface should be close to a simple Lorentzian,

$$A_p(\mathbf{k}_F,E)\sim\frac{|E|^\beta}{E^2+\text{const}\times E^{2\beta}}, \tag{31}$$

because the imaginary part of the self-energy behaves as $|E|^\beta$ with $0\leqslant\beta\leqslant 2$. On the contrary, the experimental intensity shows a pronounced minimum at the alleged Fermi-surface, Fig. 10. Taking into account the finite temperature and (or) the experimental energy resolution does not help because both of them are well below the characteristic width of the experimental spectral function in Fig. 10.

If there is indeed no Fermi-surface crossing in many cuprates, as we argue, why then does the ''maximum locus'' determination point to a large Fermi surface in cuprates, which is drastically incompatible with their kinetic and thermodynamic properties? We propose that it appears due to the fact that oxygen semiconducting band has its minima at large

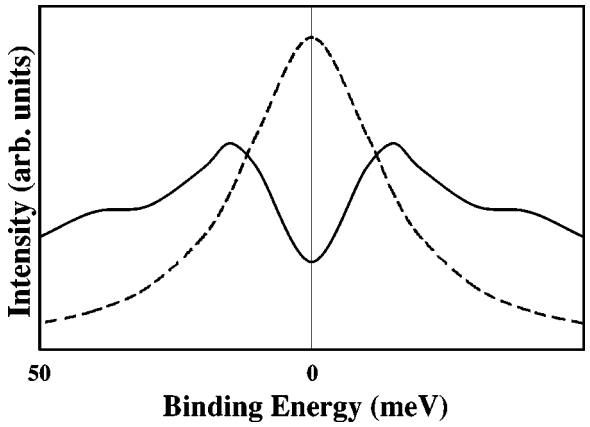

FIG. 10. The experimental ARPES signal (solid line) on the alleged Fermi surface does not correspond to a Fermi-liquid spectral function (dashed line). We assume particle-hole symmetry to obtain the spectral function for negative binding energy.

k inside or even on the boundary of the Brillouin zone. That is why ARPES show intense peaks near large **k** imitating a large Fermi surface.

VI. SUMMARY AND CONCLUSIONS

In summary, we have proposed a theory of ARPES in cuprates based on the LDA+U band structure and the bipolaron theory compatible with the normal-state kinetic and thermodynamic properties of these materials. The theory explains the narrow flatbands observed in Y123 and Y124, including their polarization, spectral and angular dependence, as well as a featureless (but dispersive) background. The ARPES peak originates from the hole excitations of the polaronic oxygen band of the buffer layers, in agreement with the experimental results and electronic structure of Schabel *et al.*[21] Differently from these authors, we suggest that this band is intrinsic for cuprates and takes part in the bipolaron formation and superconductivity, which is nicely confirmed by a few independent studies.[52] The normal-state gap is half of the bipolaron binding energy. The angular dependence of the peak and of the gap is due to the polaron band dispersion, which agrees well with the QMC results for the small Fröhlich polaron.

The spectral shape of the peak is affected by the soft lattice, spin, and random fluctuations. The characteristic scattering rate agrees well with that found in the tunneling experiments.[33] This scattering rate is temperature dependent not only due to the thermal lattice fluctuations, but also because of the anomalous screening below T_c in the charged Bose liquid.[2] The Bose-Einstein condensate screens effectively the long-range Coulomb potential of impurities. As a result, one can expect a drastic change of the damping ϵ_0 when T_c is passed. That might help to understand the near disappearance of the narrow peak above T_c in some Bi cuprates. On the other hand, in the stoichiometric Y124 with (theoretically) no impurities, one can expect about the same results from ARPES below and above T_c, which seems to be the case.[20] Within the bipolaron theory there is only one *single-particle* gap, which is half of the bipolaron binding energy both below and above T_c.

We believe that many cuprates are doped insulators with no Fermi surface at all due to the bipolaron formation. The Fermi-surface crossing, if it were firmly established in the overdoped samples, would correspond to a small Fermi surface of the oxygen band pockets located at finite **k** like in many ordinary semiconductors, for example, in Ge and Si.

ACKNOWLEDGMENTS

The authors greatly appreciate enlightening discussions with D. S. Dessau, N. E. Hussey, V. V. Kabanov, P. E. Kornilovitch, G. J. Kaye, A. I. Lichtenstein, G. A. Sawatzky, J. R. Schrieffer, Z.-X. Shen, J. Zaanen, G. Zhao, and R. Zeyher. C.J.D. has been supported in this work by a grant from the EPSRC of the UK.

[1] J.G. Bednorz and K.A. Müller, Z. Phys. B: Condens. Matter **64**, 189 (1986); Angew. Chem. Int. Ed. Engl. **27**, 735 (1988).
[2] A.S. Alexandrov and N.F. Mott, Rep. Prog. Phys. **57**, 1197 (1994); *High Temperature Superconductors and Other Superfluids* (Taylor & Francis, London, 1994); *Polarons and Bipolarons* (World Scientific, Singapore, 1995).
[3] A.S. Alexandrov, in *Models and Phenomenology for Conventional and High-temperature Superconductivity*, Proceedings of the International School of Physics ''Enrico Fermi,'' Course CXXXVI, Varenna, 1997, edited by G. Iadonisi, J.R. Schrieffer, and M.L. Chiofalo (IOS Press, Amsterdam, 1998), p. 309.
[4] For a recent review, see Zhi-xun Shen, in *Models and Phenomenology for Conventional and High-temperature Superconductivity* (Ref. 3), p. 141.
[5] D.C. Johnston, Phys. Rev. Lett. **62**, 957 (1989).
[6] K.A. Müller *et al.*, J. Phys.: Condens. Matter **10**, L291 (1998).
[7] D. Mihailovi'c *et al.*, J. Supercond. **10**, 337 (1997).
[8] J. Hofer *et al.*, Physica C **297**, 103 (1998).
[9] B. Batlogg *et al.*, Physica C **135-140**, 130 (1994); H.Y. Hwang *et al.*, Phys. Rev. Lett. **72**, 2636 (1994).
[10] J.W. Loram *et al.*, Physica C **235**, 134 (1994).
[11] C. Kendziora *et al.*, Phys. Rev. Lett. **79**, 4935 (1997).
[12] Z.-X. Shen and J.R. Schrieffer, Phys. Rev. Lett. **78**, 1771 (1997), and references therein.
[13] Ch. Renner *et al.*, Phys. Rev. Lett. **80**, 149 (1998).
[14] N.L. Saini *et al.*, Phys. Rev. Lett. **79**, 3467 (1997).
[15] N.L. Saini *et al.*, Phys. Rev. Lett. **82**, 2619 (1999)
[16] J.W. Loram *et al.*, J. Supercond. **7**, 243 (1994).
[17] H. Ding *et al.*, Nature (London) **382**, 51 (1996).
[18] M. Randeria and J.-C. Campuzano, in *Models and Phenomenology for Conventional and High-Temperature Superconductivity* (Ref. 3), p. 115.
[19] J. Mesot *et al.*, Phys. Rev. Lett. **82**, 2618 (1999).
[20] K. Gofron *et al.*, Phys. Rev. Lett. **73**, 3302 (1994).
[21] M. C. Schabel *et al.*, Phys. Rev. B **57**, 6090 (1998).
[22] A. Ino *et al.* (unpublished).
[23] C.-H. Park *et al.*, Phys. Rev. B **52**, R16 981 (1995).
[24] A.S. Alexandrov, Philos. Trans. R. Soc. London, Ser. A **356**, 197 (1998).
[25] G.A. Sawatzky (unpublished).
[26] See K. A. Müller, in *Anharmonic Properties of High-T_c Cuprates*, edited by D. Mihailovi'c, G. Ruani, E. Kaldis, and K.A. Müller (World Scientific, Singapore, 1995), p. 1; *Polarons and Bipolarons in High-T_c Superconductors and Related Materials*, edited by E.K.H. Salje, A.S. Alexandrov, and W.Y. Liang (Cambridge University Press, Cambridge, 1995).
[27] A.S. Alexandrov, Phys. Rev. B **53**, 2863 (1996).
[28] B.I. Halperin, Phys. Rev. **139**, A104 (1965).
[29] C.R.A. Catlow, M.S. Islam, and X. Zhang, J. Phys.: Condens. Matter **10**, L49 (1998).
[30] A.S. Alexandrov, Physica C **182**, 327 (1991).
[31] A.S. Alexandrov, V.V. Kabanov, and N.F. Mott, Phys. Rev. Lett. **77**, 4796 (1996).
[32] A.S. Alexandrov and G.J. Kaye, J. Phys.: Condens. Matter **11**, L15 (1999).
[33] A.S. Alexandrov, Physica C **305**, 46 (1998).
[34] D.A. Wollman *et al.*, Phys. Rev. Lett. **71**, 2134 (1993); C.C. Tsuei *et al.*, *ibid.* **73**, 593 (1994); J.R. Kirtley *et al.*, Nature

(London) **373**, 225 (1995); C.C. Tsuei *et al.*, Science **272**, 329 (1996).
[35] A.S. Alexandrov, Phys. Rev. Lett. **82**, 2620 (1999).
[36] A.S. Alexandrov and V.V. Kabanov, Phys. Rev. B **59**, 13 628 (1999).
[37] H. Fröhlich, Phys. Rev. **79**, 845 (1950).
[38] L.D. Landau, Phys. Z. Sowjetunion **3**, 664 (1933).
[39] S.I. Pekar, Zh. Eksp. Teor. Fiz. **16**, 335 (1946).
[40] I.G. Lang and Yu.A. Firsov, Zh. Éksp. Teor. Fiz. **43**, 1843 (1962) [Sov. Phys. JETP **16**, 1301 (1963)].
[41] T.D. Lee and D. Pines, Phys. Rev. **88**, 960 (1952).
[42] A.S. Alexandrov and P.E. Kornilovich, Phys. Rev. Lett. **82**, 807 (1999).
[43] A.S. Alexandrov and C. Sricheewin (unpublished).
[44] G.J. Kaye, Phys. Rev. B **57**, 8759 (1998).
[45] Y. Okimoto *et al.*, Phys. Rev. Lett. **75**, 109 (1995); Phys. Rev. B **55**, 4206 (1997).
[46] D.S. Dessau *et al.*, Phys. Rev. Lett. **81**, 192 (1998).
[47] T. Holstein, Ann. Phys. (N.Y.) **8**, 325 (1959); **8**, 343 (1959).
[48] J. Appel, in *Solid State Physics*, edited by F. Seitz, D. Turnbull, and H. Ehrenreich (Academic Press, New York, 1968), Vol. 21.
[49] *Polarons*, edited by Yu. A. Firsov (Nauka, Moscow, 1975).
[50] E.V.L. de Mello and J. Ranninger, Phys. Rev. B **55**, 14 872 (1997); **58**, 9098 (1998).
[51] Yu.A. Firsov *et al.*, Phys. Rev. B **59**, 12 132 (1999).
[52] There is strong experimental evidence for apical holes in cuprates from the site-specific x-ray absorption [M. Merz *et al.*, Phys. Rev. Lett. **80**, 5192 (1998)] and from the site-specific effect of Ba and Y substitution for Pr in $YBa_2Cu_3O_7$ [J.D. Dow, U. Howard, and A. Blackstead, Bull. Am. Phys. Soc. **43**, 877 (1998)].
[53] H.L. Frisch and S.P. Lloyd, Phys. Rev. **120**, 1175 (1960).
[54] N.F. Mott and E. Davis, in *Electronic Processes in Non-Crystalline Materials*, 2nd ed. (Oxford University Press, Oxford, 1979).
[55] S. Chakravarty *et al.*, Phys. Rev. B **58**, R559 (1998).
[56] Y.-D. Chuang *et al.*, Phys. Rev. Lett. **83**, 3717 (1999).